EUROFUSION WPPFC-PR(16) 16129

V Rohde et al.

Arc erosion of full metal plasma facing components at the inner baffle region of ASDEX Upgrade

Preprint of Paper to be submitted for publication in
22nd International Conference on Plasma Surface Interactions
in Controlled Fusion Devices (22nd PSI)

This work has been carried out within the framework of the EUROfusion Consortium and has received funding from the Euratom research and training programme 2014-2018 under grant agreement No 633053. The views and opinions expressed herein do not necessarily reflect those of the European Commission.

Arc erosion of full metal plasma facing components at the inner baffle region of ASDEX Upgrade

V.Rohde, M.Balden, and the ASDEX Upgrade Team

Max Planck Institut für Plasmaphysik, Boltzmannstr. 2, 85478 Garching, Germany

Rohde@ipp.mpg.de

INTRODUCTION:

In the standard picture of plasma wall interaction, arcs are not taken into account as erosion source: in the 80th it was shown that for carbon physical and chemical sputtering dominate and arcs are only triggered during unstable plasma phases with enhanced MHD activity [1]. On the other hand arc traces are observed in all present fusion devices. Due to the transition to metal plasma facing components (PFCs) the role of arcing on erosion has to be reconsidered again. Recent investigations in ASDEX Upgrade (AUG) show that ELMs may trigger arcs at some locations [2] and the morphology of a major fraction of dust collected can be explained by droplet production in arcs [3].

Whereas previous investigations use the typical AUG PFCs, i.e. tungsten (W) coating of 5 micron thickness on a carbon substrate [4], bulk material was investigated this time. Two different materials were selected: W as material of the ITER divertor and P92, martensitic-ferritic high temperature steel similar to EUROFER, is the latter being under discussion for DEMO.

Arcing:

In fusion devices uni-polar arcs between plasma and PFCs, orientated close to magnetic field direction, can be triggered if the voltage is in the order of 10 - 30 V, depending on the

materials and surface conditioning. High voltages across the sheath, i.e. high plasma densities (Debye length) and electron temperatures as observed during ELMs, strongly promote the ignition of arcs. Due to the current, arcs move in a magnetic field perpendicular to the field direction opposite to the JxB direction (retrograde movement). Depending on the current an arcs consists out of many spots. As the typical spot size is in the sub-micron range, localised melting produces the characteristic craters. The arc jumps from one to another single location with a higher probability to ignite close to craters of previous arcs. Finally, macroscopically visible traces, consisting out of many micron range crates are formed.

Erosion by arcing depends not only on the PFC material and plasma conditions, but also on the surface cleanliness. The type I arc moves fast and removes only material on top of the PFCs, whereas the type II arc results in erosion of material. Erosion is due to the arc plasma consisting out of the material ions and due to the ohmic power input, which causes melting of the surface material. The molten material may be moved only some microns to form craters or splashed away by the pressure of the arc plasma forming droplets.

Deposited layers on top, for example oil, can enhance the erosion rate by orders of magnitude [5]. The role of deposits for the arcing process is not completely understood, but it is assumed that the bad electrical conductivity of the deposits reduces the velocity of the arc movement. As the arc burns for a longer time at the same location, it causes stronger erosion.

Whereas arcing is observed at many tiles in AUG, significant erosion was found only in deposition dominated regions [4,6]. At the inner baffle region, layers consisting of C, B, W ,O and hydrogen isotopes reach a thickness of typical 2-3 μm [7]. Due to the shallow angle of

the magnetic field direction and shadowing effects, the thickness of the deposits varies even on one tile.

Local melting and splashing of the molten material, i.e. droplet production, is an important erosion process by arcing. Indeed huge amounts of W droplets, about 50 % of the dust collected, are observed at AUG [8]. Taking the average shot time a flux of 10^5 droplets/ s with a typical size of 2 μm can be calculated.

As mentioned above two different processes are involved in the erosion: sputtering by the plasma of the arc, the dominate process for clean surfaces as used in laboratory investigations, and melting. Consequently measurements of the erosion rate, mostly from the 80th, use a normalisation to the charge of the arcs. Taking the average deduced from different papers [9] a slightly higher erosion of W compared to Fe is expected (78 vs 61 μg/ C), which is due to the higher specific mass. The erosion by melting depends on the melting temperature, the heat effusivity of the material used and the mobilization of the molten material. As the melting temperature of W (3695 K) is much higher than for P92 (1800 K) and the effusivity is also higher (21 vs 9 kW/ (m^2K)) more molten material is expected for steel. The liquid material can solidify close to the arc producing rims, or splash away producing droplets.

Experimental:

Inserts, made out of polished W and P92 steel, were installed at the inner divertor baffle region, which is prone for arcing [4, 6] to investigate the erosion. To allow analysis in a standard SEM device the size and weight of the inserts is limited to 20*65 mm and 8 mm thickness. Two inserts are installed in each tile and 2 different tiles (Bgr 6a and 6b), which are installed side by side in poloidal direction, are used (Fig. 4). The two P92 inserts were

both mounted on the lower tile, the tungsten insert at right side of the upper one. For comparison, a tungsten sample installed at the same location as the right side P92, but during the campaign 2012, is investigated too. Polished samples are used as the surface roughness of technical materials is in the micron range similar to the typical width of arc traces. Moreover, grinding grooves possibly produced during the fabrication process influence the direction of arcs and even hinder their detection. The inserts were exposed for one experimental campaign (Dec 13 till Oct 14) for 7150 s of divertor operation and for 4747 s (Jan 12 till Sep 12).

After the opening of the vessel the tiles were removed, the inserts disassembled and a part of the samples was cleaned by wiping using deionised water to remove the deposited layers. A confocal laser scanning microscope (Olympus LEXT 4000) was used to image the surface by normal optical light microscopy and to obtain 3D topography data. Underneath the deposited layer, a large fraction of the polished surface is unaffected, which is observed at cleaned areas. Any depression beyond the polished surface is assigned as eroded. The volume of these depressions regarding a reference plane parallel to the surface and their areal fraction are obtained. To get reliable results the investigated area must be significantly greater than the arc structure. For analysis areas of 1.9*3.8 mm^2 in a torodial row across the samples are selected.

Tungsten inserts:

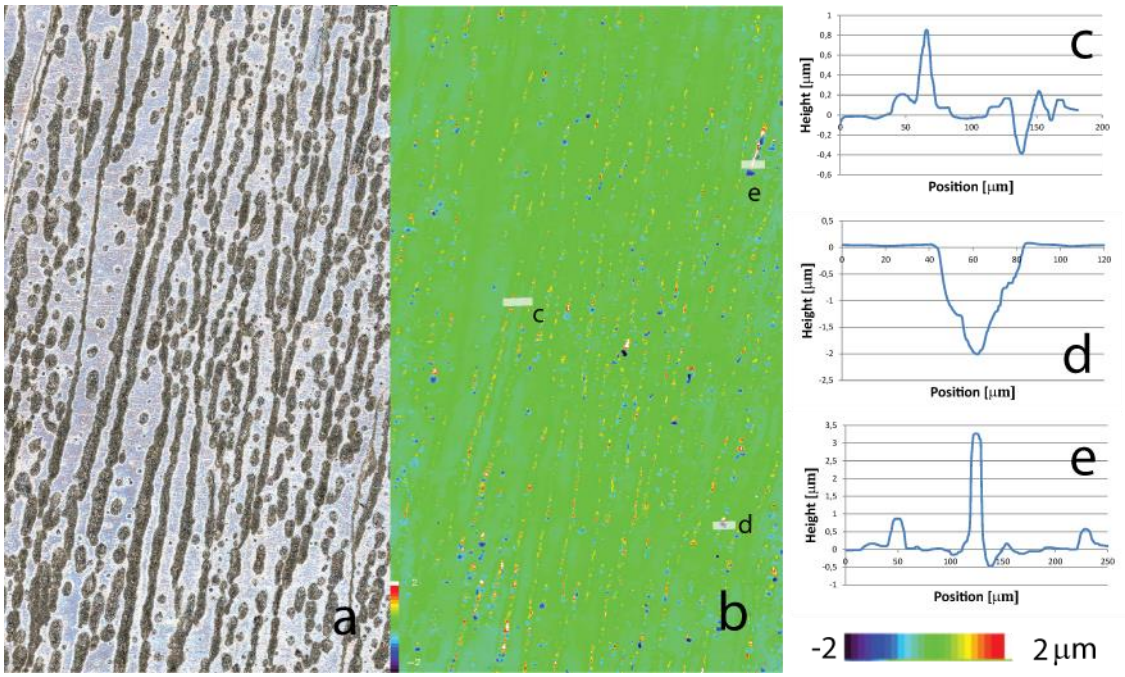

Figure 1 Picture of the W insert (2014, Positions 2) (a) showing the arc traces and obtained height map (b) of an analysis area of 1.9*3.8 mm^2 (the colour scale gives the depth). In (c-e) profiles as marked in (b) are shown.

A view on a region in the centre of the insert for the cleaned W surface is shown in Fig. 1a. The polished surface below the deposition layer is partially affected by arcing, the dark structures with the direction roughly from top to bottom. The arcs removed locally the complete deposition layer of up to 3 µm thickness (not shown in this figure). Derived from the optical picture the area affected by arcing could be estimated. Counting all pixel below half maximum intensity about 40 % of the surface is affected by arcing, but the depth map (Fig. 1b) is needed to determine the erosion. Most of the traces seen in the optical picture are also found at the depth map. Two different kinds of traces are observed: single craters (1d) and complete traces (1c,e) indicating different burning conditions for the arcing. Whereas some craters reaches depths below 2 µm (black) the typical erosion in the traces is less than 0.4 µm. Additionally, a significant amount of molten W is deposited (yellow,red) above the polished level (green) close to the erosion region.

Steel inserts:

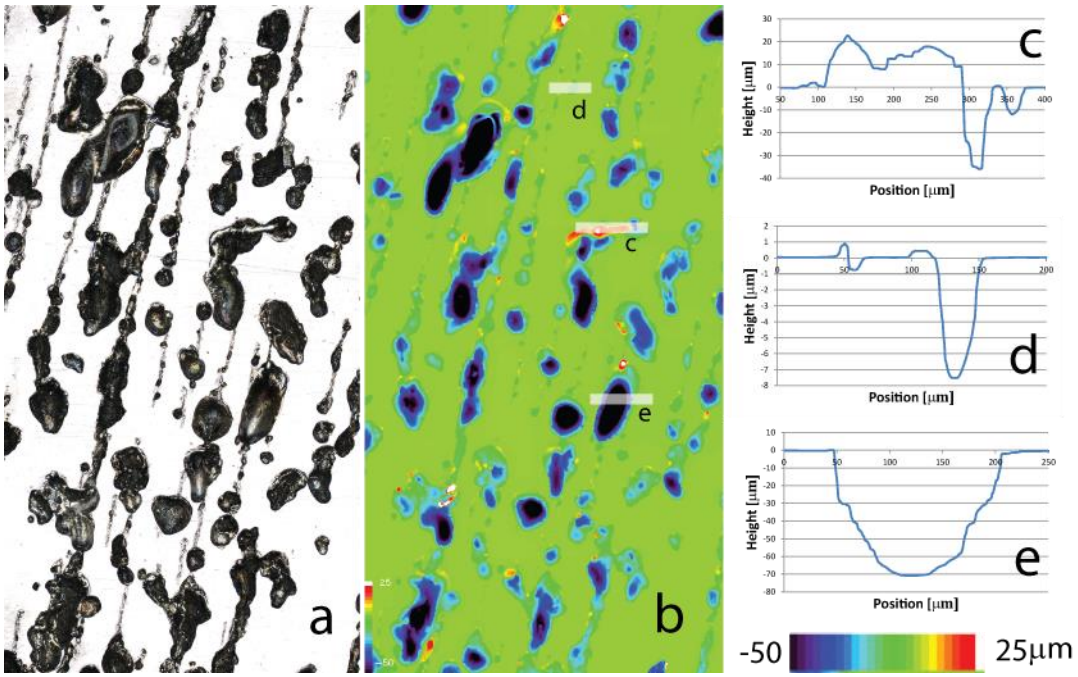

Figure 2 Picture of the P92 insert (2014, Position 2L) (a) showing the arc traces and obtained height map (b) of an analysis area of 1.9*3.8 mm mm^2 (the colour scale gives the depth). In (c-e) profiles as marked in (b) are shown. Please note the different depth scales in Figs. 1 and 2.

An equivalent region as for W is analysed and shown in Fig. 2 for P92 steel. Again the arcs erode the substrate below the deposition layers. Using the same criterion as above for the optical picture about 35 % of the surface is affected by arcing. The number of arc traces is slightly lower than for W. Beside the long arc traces (2d) also craters (2e) are present. But in contrast to the W surface the respective craters are much bigger with about 100 µm diameter and about 50 µm deep. Note the depth scale in Fig. 2b is more than one order of magnitude larger than in Fig. 1b. These craters dominate the erosion. Close to deep craters solidified steels forms rejects (Fig. 2c). The bigger craters and rejects are also visible in the non-cleaned areas. Whereas some smaller craters are filled with deposits, which were not removed by the cleaning technique used, the deep craters show mostly clean metal surface at the ground. An interesting detail of the measurements is the direction of the arc traces: As P92 can be

magnetized, the local magnetic field is influenced by the probes themselves. For this reason the direction of the arc traces, which are orientated perpendicular to the magnetic field, bends close to the edges of the probes.

Evaluation:

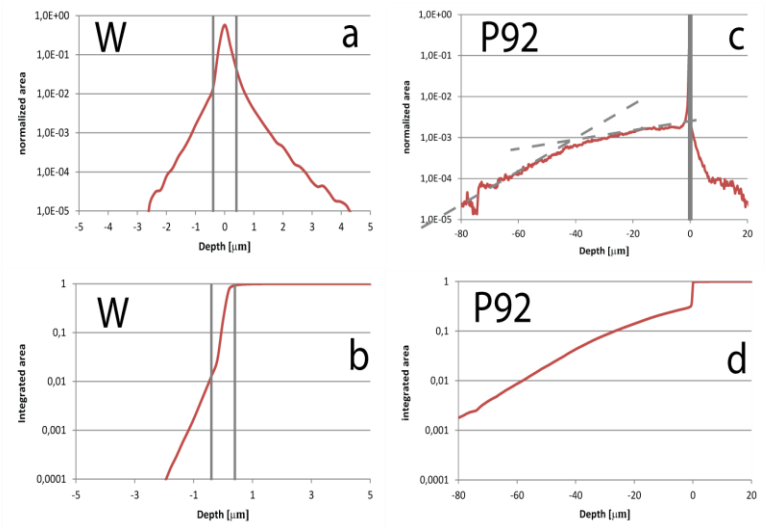

Figure 3 Distribution functions of the data presented in Figs. 1 and 2 for W (a,b) and P92 (c,d)

The gathered depth maps with a spatial resolution of 0.6*0.6 μm^2 were first used to determine the unaffected surface position and correct the data for tilting of the probe. Then the number of pixels was counted to determine the total area eroded down to a certain depth. In Fig. 3 the distribution functions, normalised to the total analysed area, are shown for tungsten and for P92. For tungsten an almost logarithmic decay reaching depths down to 3 µm are observed. The region close to the original surface is affected by deposits, melt layers from arcing and the accuracy of the polished surface. As the amount of eroded material depends on the depth below the surface a criterion has to be defined to define the

unaffected surface. From Fig. 3 a clear bend in the decay length is found at -0.4 μm. As shown in Fig. 1a large fraction of the surface is affected by arc traces, resulting in the broad peak between -0.4 and 0.4 μm in the depth profiles. As the distribution function is almost symmetric in this depth range rearrangement is dominate. The fraction above 0.4 μm is due to deposits. Physically these areas are effected by arcs, which produce rims (Fig. 1 c) at the side of the traces, but cause no significant erosion, as for example droplet production. EDX investigations yield that they consists out of C, B, O, and W, i.e. the layers on top are mixed together. To determine the erosion of tungsten by arcing one has to distinguish between mobilized material which is redeposited close to the arc spots and material, which is lost. As shown in Fig. 3b, the depth, which is defined as reference level strongly effects the amount of tungsten, which is eroded. In the following only depth of < -0.4 μm below the reference level were counted as eroded material.

P92 shows a more complicated behaviour with a shoulder down to 10 μm and a logarithmic decay below this. Craters down to 80 μm are found on the P92 probe. Similar as for tungsten mixed deposits are found. Three solidified molten iron structures with heights up to 30 μm are found on this sample, resulting in the shoulder in Fig. 3c above 20 μm.

Taking the integrals of this distribution functions (Fig. 3b), three different areas could be identified for W. About 3.3 % of the surface is deposition dominated ($> +0.4$ μm), mostly by the rims close to the arc traces. The major part of the surface (-0.4 μm to +0.4 μm) shows no net erosion, even if the visual picture shows huge arc traces and the region below -0.4 μm (2.7 % of the total surface), which counts for the erosion.

Taking the same criterion as above for the P92 sample only 2 % of the surfaces is above the level of 0.4 μm. The unaffected area is much closer to the visual pictures. About 46 % of the surface shows erosion below a level of -0.4 μm.

To determine the amount of erosion, different areas in toroidal direction were measured and evaluated on each insert. The volumes of the depressions below a reference plane parallel to the surface were determined for various distances to the surface level. These volumes normalised to the total area analysed, presenting the average erosion, had been normalised to the total lower divertor operation time during the exposure. To clarify the different deposition and erosion depths of W and P92 the results for different levels are plotted in Fig. 4. The areas shown above are the column 2 in Fig 4b for WbR and position 2 in Fig 4c for P92aL.

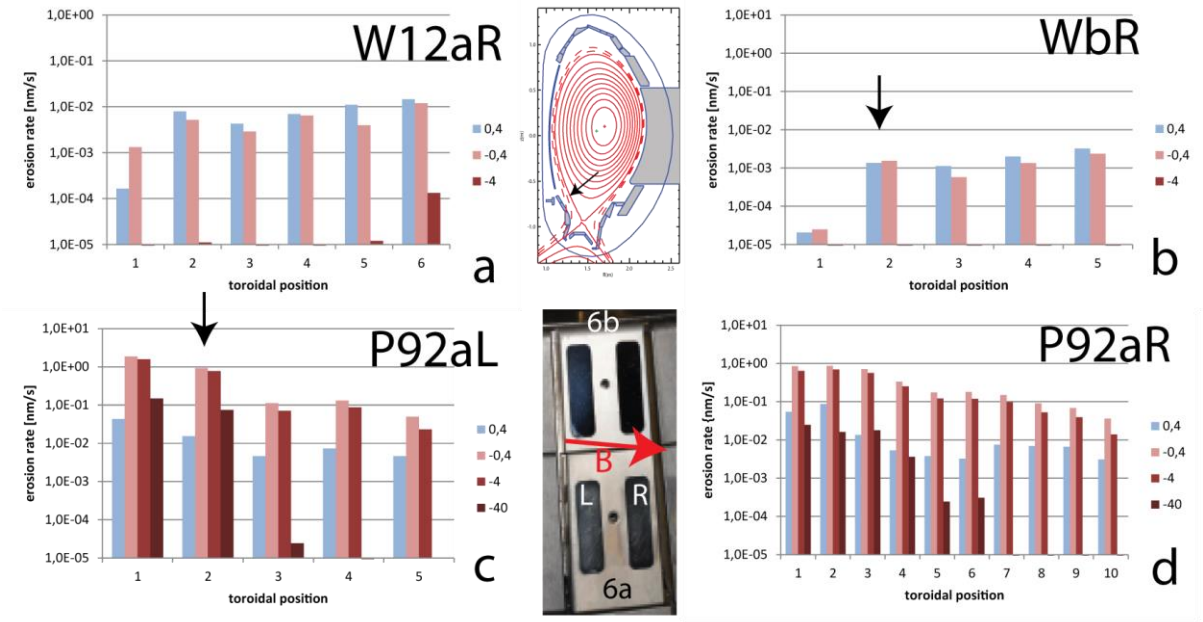

Figure 4 Toroidal profiles of the time averaged erosion rates for the inserts investigated. In blue deposition above a level of 0.4 μm is shown. Erosion rates for different levels are painted in red. The central pictures show the positions of the inserts.

The tungsten inserts were both installed on the right side, but on the different tiles. On the insert itself, a similar behaviour is found for both W probes. For the first position quite low erosion is found as this part is protected by a tile to avoid a leading edge. The deposition and erosion show a slight increase by a factor of 2 to the right side of the insert. Only for the deepest craters (< - 4 μm) an increase by a factor of 10 is found. The average deposition and erosion is by a factor of 5 higher at the lower tile (6a). This comparison points to the local conditions, which strongly influence the arcing.

For the P92 inserts, installed at the same tile but on the different positions, the right probe shows 30 % more deposition as the left one, i.e. they are almost similar. But the erosion at the left tile is twice compared to the right insert. Again the profiles across the P92 inserts are similar for both, but the trend is invers compared to the tungsten ones: the strongest erosion

is found on the left side of the insert with a strong decrease by a factor of 30 in toroidal direction. For the deepest craters this decrease is even stronger as values below 50 μm are only observed on the left side of the insert. The orientation of the arc traces can be used to determine the local magnetic field, as arcs have to move perpendicular. This orientation changes significant close to the probe edge, were the deep craters are found. Local changes of the magnetic field due to the ferromagnetic nature of the material, seems to play a role in the erosion.

Due to the local variations data obtained at the same position, but in different campaigns, are used to compare tungsten with P92. Taking the average of all measurements on the insert the deposition found is quite similar for both materials (W: 0.008 nm/ s, P92: 0.019 nm/ s). Taking average on the insert the erosion of P92 is 65 times larger than for tungsten (W: 0.005 nm/ s, P92: 0.340 nm/ s). First evaluations, using a subset of the data presented, yield an erosion of P92 about 30 times stronger compared to tungsten [10]. This difference points to the importance of the definition of the depth which is defined as reference level. For P92 deep craters are found, i.e. a change of the reference level has only a minor effect on the erosion rate. The picture is different for tungsten, where most of the surface is affected by the arcs, but the depth is mostly below 0.4 μm. A reference level in this range, which is shown to be dominated by redistribution but not net erosion, will enhance the seemingly erosion rate.

As the erosion by arcs shows a strong local variation, it is also worth to discuss the maximal erosion measured. Taking the analysis areas of 1.9*3.8 mm^2 a maximal average erosion of 1.9 nm/ s is found for P92, compared to 0.01 nm/ s for tungsten. Evaluation of the depth profiles clarifies the different behaviour of the two materials: whereas for tungsten only a fraction of 0.004 % is eroded below 4 μm, 9 % of the P92 surface shows erosion below 40 μm.

For comparison the same tile and location are used, as strong local variation of the erosion complicates an extrapolation of the material release rate. Taking the minimum and maximum value for the analysis areas an erosion for W between $0.8*10^{13}$ W at $cm^{-2}s^{-1}$ and $7.5*10^{13}$ W at $cm^{-2}s^{-1}$ and for P92 between $30.0*10^{13}$ Fe at $cm^{-2}s^{-1}$ and $730.0*10^{15}$ Fe at $cm^{-2}s^{-1}$ is determined. Even as the position of the probes is deposition-dominated, significant erosion is observed, which can be compared with the erosion at the outer divertor strike line of $70*10^{13}$ at $cm^{-2}s^{-2}$ for W [7].

As discussed above this big difference of the erosion for W and P92 is not expected from the erosion yield for arcing given in literature [9]. All literature data are for clean surfaces but in AUG the strong erosion is correlated with deposits. The influence of these layers is still not completely understood, and laboratory investigations would be beneficial. A hypothesis to explain the high erosion for P92 is the production of droplets, which increases strongly, as the material temperature reaches the melting point. The lower effusivity and melting temperature for P92 may explain this behaviour. To understand the droplet production and the effect of the physical properties, a set of different polished probes was installed for the ongoing (2015/ 16) experimental campaign of AUG. To scan different melting points and effusivities, this set comprises probes from Al, Cu, Cr, SS, P92, Mo and W.

Conclusion:

At the inner baffle of the AUG divertor massive polished inserts of tungsten and P92 steel were installed to measure the erosion by arcing. As this region is deposition dominated the deposits were removed by wiping to allow measurements at the insert itself. Whereas in the optical picture typically a third of the surface is affected for both inserts, depth profiles show strong differences. For tungsten most of the traces are less than 0.4 μm deep and a similar

amount of tungsten is deposited close to the traces. These arcs show only a redistribution but no net erosion. One a few craters up to 4 μm resulting in an average erosion rate of $2*10^{13}$ at $cm^{-2}s^{-2}$ are observed. The behaviour for P92 steel is quite different: most of the traces are 4 μm deep, up to 80 μm were observed. The average erosion rate of $400*10^{13}$ at $cm^{-2}s^{-2}$, i.e. more than a factor of hundred higher compared to tungsten. To get an idea for the relevance the erosion rates the erosion by arcing at the inner baffle is compared with the tungsten erosion at the outer strike point, the region with the highest erosion rate at AUG. As the baffle region is 7 times larger than the strike point region the tungsten release by arcing is 25 % of the strike point erosion. For a full P92 steel baffle region about 45 times more iron will be released than tungsten from the outer strike point. Therefore, erosion by arcing has to be taken into account to determine the optimal material mix for future fusion devices. For Be the melting temperature is close to the steel, but the effusivity is even higher than for W, which complicates predictions. Further investigations, using different materials are started at AUG to disentangle the different effects and to allow estimating the droplet production by arcing.

References

[1] McCracken, J.Nucl.Mat. , 93, (1980), 3

[2] Rohde et al., J.Nucl.Mat. , 415, (2011), S46

[3] Endstrasser et al., J.Nucl.Mat. , 415, (2011), S1085

[4] Rohde et al., J.Nucl.Mat. , 438, (2013), 800

[5] Mioduszewski,Nucl.Fusion, Data Compendium for Plasma-Surface Interactions, 1984

[6] Herrmann et al., J.Nucl.Mat. , 390, (2009), 747

[7] Mayer et al., Phys.Scr. , T138, (2009), 014039

[8] Balden et al., Nucl.Fusion , 54, (2014), 073010

[9] Post, Behrisch , Physics of Plasma-Wall interactions in Controlled Fusion,

ISBN 0-306-42097-XJ

[10] Rohde et al., EPS 2015, http:/ / ocs.ciemat.es/ EPS2015PAP/ pdf/ P1.119.pdf